



Nanotwin formation in Ni–Mo–W alloys deposited by dc magnetron sputtering

Gianna M. Valentino^a, Pralav P. Shetty^b, Ankur Chauhan^a, Jessica A. Krogstad^b, Timothy P. Weihs^c, Kevin J. Hemker^{a,c,*}

^a Department of Mechanical Engineering, Johns Hopkins University, Baltimore, MD 21218, United States

^b Department of Materials Science and Engineering, University of Illinois Urbana-Champaign, Urbana, IL 61801, United States

^c Department of Materials Science and Engineering, Johns Hopkins University, Baltimore, MD 21218, United States

ARTICLE INFO

Article history:

Received 6 March 2020

Revised 3 May 2020

Accepted 11 May 2020

Available online 5 June 2020

Keywords:

Sputtering

Nanoindentation

Hardness

Nanotwins

Deposition rate

ABSTRACT

Nanotwinned metals and alloys have an attractive suite of properties, but the formation of the underlying nanostructure is generally dependent on the alloy chemistry and processing conditions. This study was undertaken to investigate the effect of deposition rate on nanotwin formation in sputter deposited $\text{Ni}_{84}\text{Mo}_{11}\text{W}_5$ that possess ultrahigh strength and stability. Deposition rates of 0.5–2.3 nm/s were examined and the grain size, texture, twin spacing and hardness were characterized. Minimal variations in the underlying nanostructure and attendant hardness were observed, elucidating a wide processing window and the importance of chemistry on the formation of nanotwins in this alloy.

© 2020 Acta Materialia Inc. Published by Elsevier Ltd. All rights reserved.

The recent synthesis of Ni–Mo–W films has shown an extraordinary balance of thermal, mechanical and electrical properties, underpinned by the formation of growth nanotwins [1,2]. In addition to this suite of properties, Ni–Mo–W possesses a lower and tailorable coefficient of thermal expansion [3] and is compatible with wafer-level manufacturability of metal microelectromechanical systems (MEMS) devices [4]. However, the processing window for depositing nanotwins in Ni–Mo–W alloys is not clear from the earlier work.

Nanotwinned face-centered cubic (fcc) metals have received considerable attention in recent years due to their high strength, promising balance of properties and microstructural stability as compared to nanocrystalline metals. Growth nanotwins have historically been observed in low stacking fault energy (SFE) fcc metals and alloys, with most studies focused on nanotwinned Cu. The development of very fine nanotwins with the ability to control twin thickness has enabled an optimization of strength, ductility and electrical conductivity at intermediate thicknesses [5–7]. Lu et al. showed that it was possible to decrease the nanotwin thickness in electrodeposited Cu by either increasing the deposition rate or by decreasing the SFE through alloying with Al or Zn [8].

Electrodepositing complex alloys with the requisite chemistry and minimal impurities can be challenging. Alternatively, sputter deposition has been used to deposit multicomponent Ni-base superalloys with desired chemistries [9,10]. Pure Ni has a high SFE that generally inhibits the formation of nanotwins, although a few investigators have reported growth twin formation in Ni films that were deposited at very high rates via pulsed electrodeposition (8–17 nm/s) [11], sputter deposition (12.5–30 nm/s) [12,13] or when using an electrodeposition-sputtering hybrid technique [14]. The twin distribution in the sputtered pure Ni films [12,13] was highly sporadic, in contrast to $\text{Ni}_{83.6}\text{Mo}_{14}\text{W}_{2.4}$ (at.%) films that were sputter deposited at a moderate rate (3.2 nm/s) and shown to have a high density of nanotwins with a strong {111} texture and an impressive suite of properties [1,2].

The role of sputter deposition rate on nanotwin formation in Ni–Mo–W alloys was unknown, therefore, this study was undertaken to identify the processing window for reliably reproducing the underlying nanostructure and to determine if it is possible to tailor the nanotwin spacing, similar to nanotwinned Cu [8,15–17]. A fixed alloy chemistry of $\text{Ni}_{84}\text{Mo}_{11}\text{W}_5$ was sputter deposited at deposition rates between 0.5 and 2.3 nm/s to determine how the variation of deposition rate affects the nanotwin formation, the defect density and the mechanical behavior. Two different magnetron sputtering chambers were used to expand the range of accessible direct current (dc) power and therefore deposition rates. A custom sputtering system deposited films at room temperature with

* Corresponding author at: Department of Mechanical Engineering, Johns Hopkins University, Baltimore, MD 21218, United States.

E-mail address: hemker@jhu.edu (K.J. Hemker).

Table 1

Summary of the deposition conditions used for the $\text{Ni}_{84}\text{Mo}_{11}\text{W}_5$ (at.%) films, all deposited at room temperature.

Power [W]	Ar pressure [mTorr]	Film thickness [μm]	Duration [min]	Deposition rate [nm/s]
200	1.0	2.7 ± 0.1	85	0.5
400	1.0	2.6 ± 0.3	60	0.7
600	1.0	2.3 ± 0.2	40	0.9
2500	1.0	21.1 ± 0.2	150	2.3

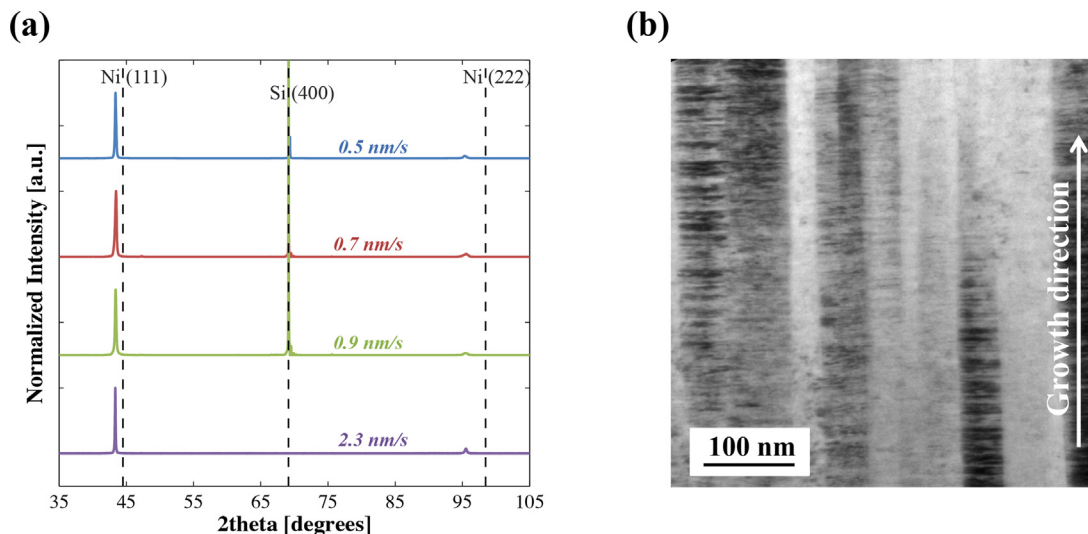


Fig. 1. (a) XRD data of the Ni–Mo–W films across the deposition rates, with polycrystalline Ni peaks (black dashed lines) shown for reference. Intensity is normalized to the (111) peak for comparison and a strong (400) Si peak is evident for the films attached to their substrate. (b) Representative low magnification bright field micrograph from the films deposited at 0.5 nm/s, indicating a high density of nanotwins distributed throughout all grains.

a rate of 2.3 nm/s using dc power of 2500 W, argon (Ar) sputtering gas pressure of 1.0 mTorr and a base pressure of 10^{-7} Torr. A combinatorial target with $\text{Ni}_{85}\text{Mo}_{15}$ and $\text{Ni}_{85}\text{W}_{15}$ wedges produced films with a compositional spread, as detailed elsewhere [3], and $\text{Ni}_{84.4}\text{Mo}_{10.7}\text{W}_{4.9}$ films were used for this study. Additional films were deposited using a 3-inch single alloy target of $\text{Ni}_{84}\text{Mo}_{11}\text{W}_5$ and a commercial sputtering chamber AJA International Inc. ATC 1800 UHV. The $\text{Ni}_{84}\text{Mo}_{11}\text{W}_5$ films were deposited onto 4-inch (100) Si wafers at room temperature with deposition rates of 0.5, 0.7 and 0.9 nm/s and a base pressure of 10^{-7} – 10^{-8} Torr. The dc power was varied from 200 to 600 W while the Ar pressure was held constant at 1.0 mTorr. Table 1 summarizes the deposition conditions that were investigated.

X-ray diffraction (XRD) scans of all four as-deposited Ni–Mo–W films showed a dominant peak at 43.4° and a much smaller peak at 95.6° , which corresponds to a single-phase fcc crystal structure with a lattice parameter of 3.61 Å and very strong {111} texture. Fig. 1a displays the XRD profiles normalized to the (111) peak for ease of comparison. The measured (111) and (222) peaks display a shift from the polycrystalline Ni diffraction peaks, indicating a lattice expansion associated with the incorporation of Mo and W solute atoms into the Ni lattice. The films sputtered at 2500 W were thicker than those sputtered at lower powers because of their higher deposition rate and longer sputter duration (Table 1). After deposition, the thicker films deposited at 2500 W were removed from their substrate and investigated as freestanding films. All other films were characterized on their Si substrate, which is evident from the strong (400) Si peak observed in Fig. 1a.

Cross-sectional TEM foils were prepared by focused ion beam (FIB) lift-out using a FEI Strata DV235 Dual-Beam and a FEI Helios G4 U. A representative low magnification bright field micrograph of a film deposited at the lowest deposition rate of 0.5 nm/s (Fig. 1b) reveals a highly columnar microstructure with a high density of

nanotwins within each grain. All grains showed fully nanotwinned structures with similar densities across the investigated deposition rates. Higher magnification bright field TEM images and selected area electron diffraction (SAED) patterns were employed to investigate the nanotwinned microstructure in the as-deposited films. As shown in Fig. 2, tall columnar grains were observed parallel to the growth direction and SAED patterns confirmed very high densities of nanotwins oriented perpendicular to the growth direction. For example, the insets in Fig. 2a–d were all indexed for the matrix and the twin orientations. Notable streaking of the diffraction spots is indicative of the presence of stacking faults, which were confirmed by high-resolution TEM micrographs that showed a modest number of stacking faults relative to the number of twins. The bright field micrographs allowed for direct measurement of the thickness of more than 100 twins in multiple grains, with the distributions illustrated in Fig. 3. All deposition rates were found to have a distribution of finely spaced nanotwins below 11 nm. Their average values are shown in Table 2. The average twin thickness was found to be less than 4 nm across all deposition conditions with minimal variations as a function of deposition rate.

TEM-based automated crystal orientation mapping (ACOM) confirmed the strong {111} out-of-plane texture across all deposition conditions, as illustrated in Fig. 4, and provided a direct measure of the in-plane columnar grain diameters. The in-plane TEM specimens were prepared using Ar ion milling with liquid nitrogen to prevent heat-induced damage caused by the ion bombardment. The grain size measurements displayed in Table 2 are averaged from two separate $1.3 \mu\text{m} \times 1.3 \mu\text{m}$ ACOM maps for each deposition rate. A modest increase in average grain diameter is observed with increasing deposition rate. While the increases fall within one standard deviation of each other, we observe a constant trend toward larger diameters. During film deposition, atoms are quenched onto the substrate surface with high energy and low surface mo-

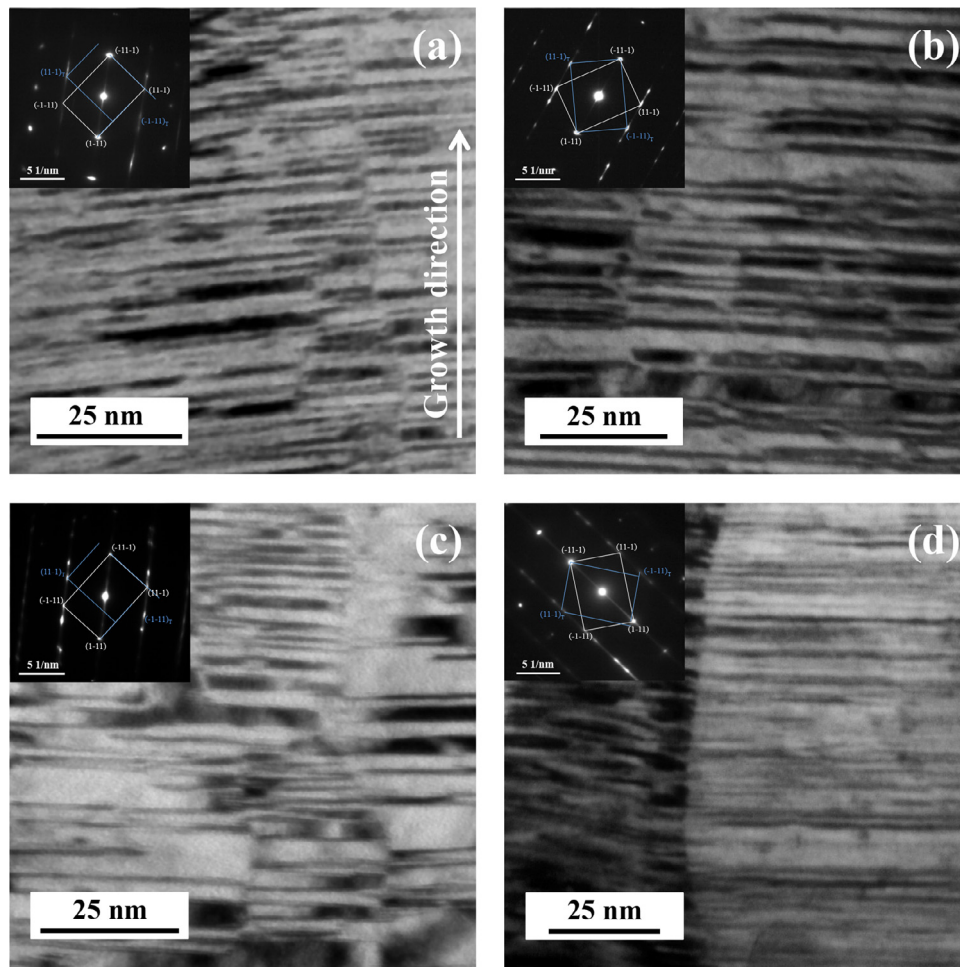


Fig. 2. Bright field TEM micrographs of the films sputtered at (a) 0.5, (b) 0.7, (c) 0.9 and (d) 2.3 nm/s with vertical growth direction. Insets of SAED patterns on the [011] zone axis are indexed for twin and matrix orientations.

Table 2

A summary of the in-plane grain size, nanotwin thickness, hardness and estimated compressive yield strength as a function of deposition rate.

Deposition rate [nm/s]	In-plane grain size [nm]	Twin thickness [nm]	Hardness [GPa]	Compressive yield strength [GPa]
0.5	58.4 ± 30.5	3.2 ± 1.3	9.9 ± 0.2	3.3 ± 0.1
0.7	65.5 ± 39.1	3.7 ± 1.9	9.4 ± 0.2	3.1 ± 0.1
0.9	74.5 ± 31.5	3.4 ± 1.8	9.8 ± 0.2	3.3 ± 0.1
2.3	88.8 ± 38.6	3.3 ± 1.7	10.2 ± 0.7	3.4 ± 0.2

bility. As sputtering continues, a modest amount of heat builds up, increasing the overall substrate temperature. Increasing the deposition rate provides higher energy for the atoms impinging on the surface, causing more substrate heating when compared to the lower rates. Thornton has shown that films sputtered at a low homologous temperature (T/T_m) have an increase in columnar width as the temperature increases [18,19], as reported in Table 2.

Instrumented nanoindentation and the Oliver–Pharr method [20] were used to measure hardness. A 50 mN load cell on the iNano instrument (NanoMechanics Inc.) with a diamond Berkovich indenter tip was used to make 20 indents per film at a constant indentation strain rate of 0.2 s^{-1} . Hardness values were averaged between depths of 200 and 250 nm to minimize the substrate and surface roughness effects. Table 2 lists the average hardness (H) for all deposition rates, and the widely employed relation, $H = 3\sigma_y$, was used to estimate the compressive yield strength (σ_y) of each film. The estimated strength of the nanotwinned $\text{Ni}_{84}\text{Mo}_{11}\text{W}_5$ films

was found to be greater than 3.1 GPa when averaged over all deposition rates, which is similar to what was reported for more Mo-rich $\text{Ni}_{83.6}\text{Mo}_{14}\text{W}_{2.4}$ films [1,2] and to the micropillar compressive strength reported for $\text{Ni}_{84}\text{Mo}_{11}\text{W}_5$ [21]. These yield strengths are more than 2–3x higher than that of sputter deposited [12] or electroplated [11] Ni with sporadic nanotwins and even 1.5x higher than sputter deposited Ni-base superalloy 718 [22]. The strength of the nanotwinned Ni–Mo–W films is also 2–3x higher than what has been reported for other nanostructured materials, such as nanocrystalline Ni [23] and nanotwinned Cu [5,7,24].

Neither the twin spacing nor the hardness were found to depend on the rate at which the nanotwinned $\text{Ni}_{84}\text{Mo}_{11}\text{W}_5$ films were deposited; the twin thickness and hardness data were both statistically invariant with rate. We note that Ott et al. investigated the effect of deposition rates (1.5–5.4 nm/s) on twin thickness in sputtered Ag films, finding that there were no changes in twin thickness with rate, but there was a change in twin density

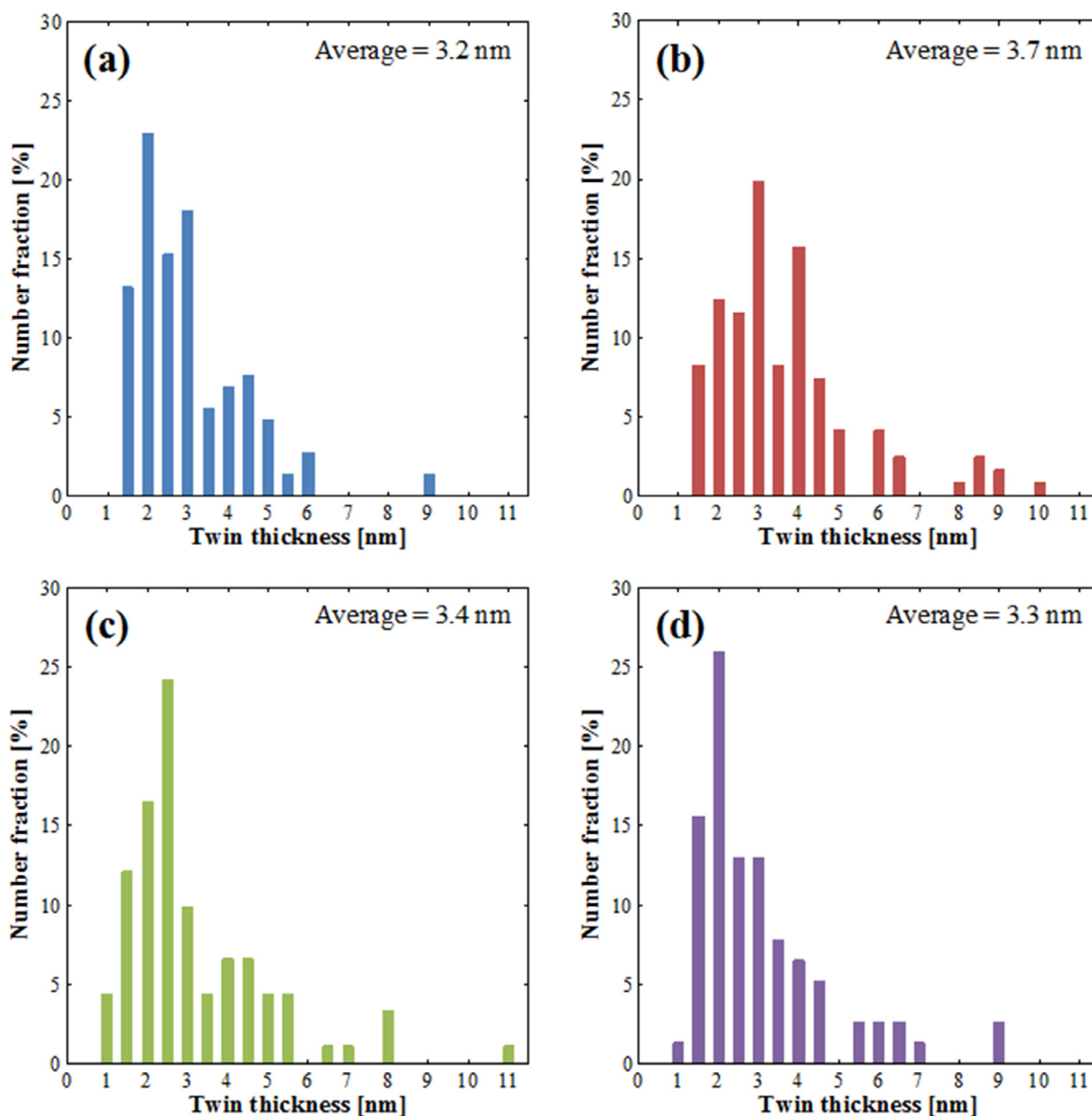


Fig. 3. Distribution of nanotwin spacing for films sputtered at (a) 0.5, (b) 0.7, (c) 0.9 and (d) 2.3 nm/s.

and texture that contributed to a variation in strength [25]. At the lower deposition rates, they found more randomly textured grains with less twin density across the films, contributing to a decrease in strength [25]. The same phenomenon was not observed in the $\text{Ni}_{84}\text{Mo}_{11}\text{W}_5$ alloy deposited in this study at even lower rates of 0.5–0.9 nm/s. The XRD results in Fig. 1a shows consistent strong {111} texture, without any other diffraction peaks present. Similar texture was observed in the inverse pole figure (IPF) maps shown in Fig. 4 and quantified using the pole figure (PF) for each ACOM scan in the inset of Fig. 4, suggesting that the $\text{Ni}_{84}\text{Mo}_{11}\text{W}_5$ films have robust texture stability over the range of deposition conditions investigated. Similarly, the high density of finely spaced nanotwins and the high hardness values suggest that the underlying nanostructure is distributed throughout the columnar grains for all deposition conditions. Thus, this $\text{Ni}_{84}\text{Mo}_{11}\text{W}_5$ alloy has a broad stability range (0.5–2.3 nm/s) for nanotwin formation, where the grains remained strongly {111} textured with high twin density and hardness.

The mechanistic reason behind this broad stability range for nanotwin formation deserves further attention. Shang et al. performed first-principles calculations for 26 different alloying elements with Ni and found that Mo and W were two of the most effective elements in reducing the SFE of pure Ni, which is reported as 130 mJ/m² [26]. For binary $\text{Ni}_{71}\text{X}_{29}$, the DFT simulations suggest that alloying with Mo and W reduces the SFE to 102 mJ/m² and 104 mJ/m², respectively [26]. In comparison, low SFE materials such as silver and copper have a SFE of 17–22 mJ/m² [27–29] and 40–78 mJ/m² [27–31], respectively. Zhang et al. developed an analytical model to understand growth twin formation during physical vapor deposition processes, where the vapor phase condenses on the surface of a substrate to form a solid film [32]. The critical radius of a disc-shaped nucleus can be calculated from that of a defect-free nucleus (r_{perfect}^*) and a twinned nucleus (r_{twin}^*). Zhang et al. considered a relative radius difference of 5% to be favorable for significant twin formation in stainless steel [32]. The relative difference can be written in terms of the twin boundary energy

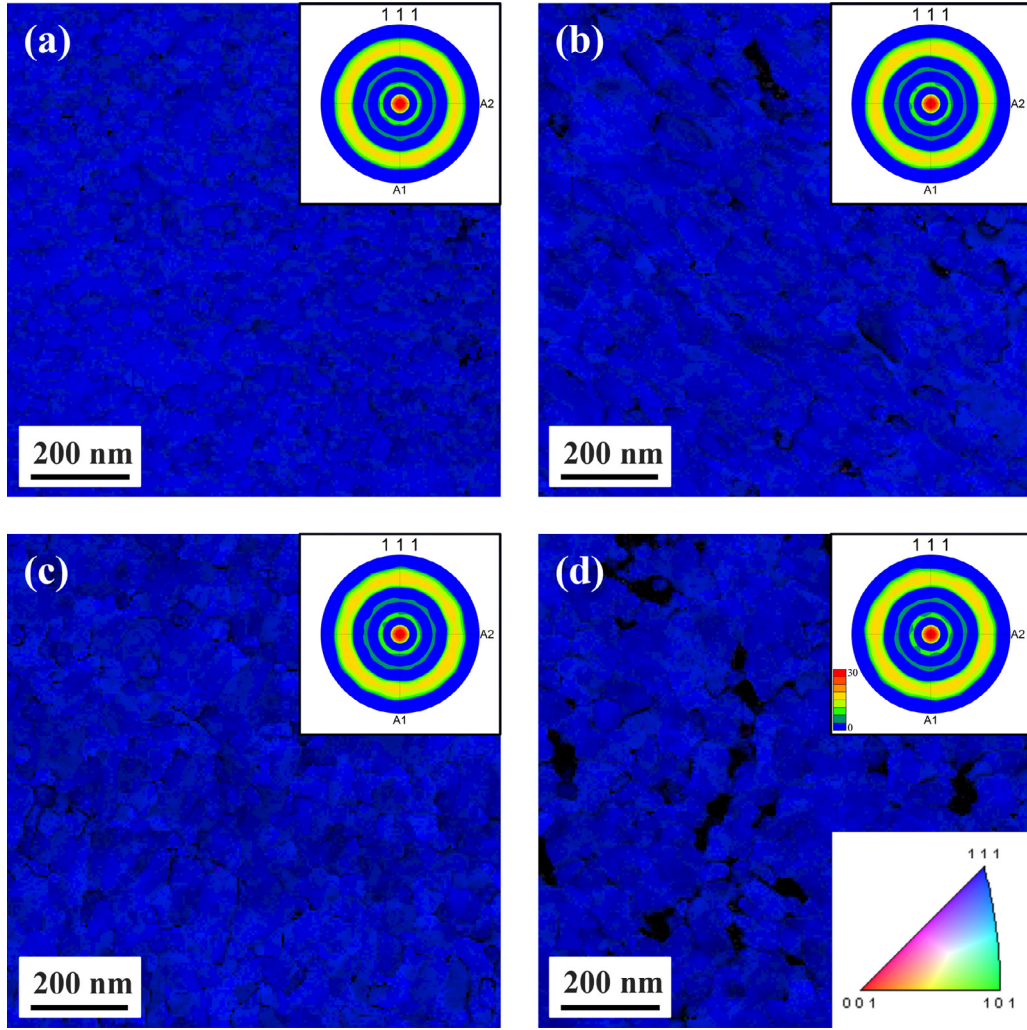


Fig. 4. IPF mapping overlaid with the confidence index, showing strong {111} texture oriented out-of-plane (parallel to the growth direction) for films sputtered at (a) 0.5, (b) 0.7, (c) 0.9, and (d) 2.3 nm/s. Insets of PFs quantifying the highly textured {111} out-of-plane columnar grains.

(γ_t , half of the SFE [29]), the {111} interplanar spacing (h), the Boltzmann constant (k), the sputtering temperature (T), the atomic volume (Ω), the deposition flux (J), the atomic mass (m) and the vapor pressure above the solid (P_s).

$$\frac{\Delta r}{r} = \frac{r_{\text{twin}}^* - r_{\text{perfect}}^*}{r_{\text{perfect}}^*} = \frac{\gamma_t}{h \frac{kT}{\Omega} \ln \left(\frac{J \sqrt{2\pi m k T}}{P_s} \right) - \gamma_t} \quad (1)$$

The widespread formation of twinned nuclei is favorable when the relative radius difference in Eq. (1) is minimized by either low SFE, high deposition flux (~deposition rate) and/or high deposition temperature.

In the current study, all $\text{Ni}_{84}\text{Mo}_{11}\text{W}_5$ films have the same SFE and were deposited at the same temperature (room temperature), with low to moderate deposition rates (0.5–2.3 nm/s). The temperature and alloy chemistry were held as experimental constants to isolate the effect of deposition rate on nanotwin formation, twin spacing and twin density. It is clear from the experimental results that $\text{Ni}_{84}\text{Mo}_{11}\text{W}_5$ films have a high density of finely spaced twin boundaries and consistently high hardness across all deposition rates. Because the deposition rate has little effect on these properties, this suggests that either the SFE of $\text{Ni}_{84}\text{Mo}_{11}\text{W}_5$ is significantly reduced compared to that of pure Ni or the critical relative radius difference is larger than 5%, either of which would facilitate abundant nanotwin formation for all the deposition rates included in

this study. This point is consistent with the observations of Wang and Dahlgren, who sputter deposited Ni at 200 °C with an average deposition rate of 12.5 nm/s and found that growth twins (170 nm) formed locally throughout the film but did not have widespread uniformity [13]. Their high deposition rate and high temperature should have promoted widespread twin formation, but only sporadic twins were observed and all of their twins had significantly larger twin spacing than those seen for $\text{Ni}_{84}\text{Mo}_{11}\text{W}_5$ films. Although not shown in the current study, extensive nanotwin formation was found across the compositional range of $\text{Ni}_{85}\text{Mo}_x\text{W}_{15-x}$ [1–4], with similar nanotwin spacing and density as shown in $\text{Ni}_{84}\text{Mo}_{11}\text{W}_5$ films. Taken as a whole, these findings suggest that alloy chemistry has an important role in widespread twin formation in Ni, through the modification of the SFE.

To better quantify the SFE of $\text{Ni}_{84}\text{Mo}_{11}\text{W}_5$, Eq. (1) can be used to estimate the critical SFE needed for favorable twin nucleation. In the deposition rate range of 0.5–2.3 nm/s, a SFE of 36–46 mJ/m² is required to satisfy the 5% relative radius criterion. If, as suggested by first-principles calculations for the binary alloys [26], the SFE was taken to be 100 mJ/m² then the relative radius criterion would have to be relaxed to 15% to predict $\text{Ni}_{84}\text{Mo}_{11}\text{W}_5$ nanotwin formation. This range of parameters is consistent with the fact that nanotwins are commonly observed in Cu and with Velasco et al.'s observation that Cu–Al alloys with reduced SFE result in prolific nanotwin formation [16,17]. Future first-principles calculations of

Ni–Mo–W ternary alloys would lead to a greater understanding of the interplay between SFE and twin nucleation.

In summary, $\text{Ni}_{84}\text{Mo}_{11}\text{W}_5$ films were deposited in a 4.6x range of deposition rates, 0.5–2.3 nm/s, and characterized to determine the effect of deposition rate on the nanotwin formation, the attendant microstructural features and the mechanical response. All films were highly {111} textured in the growth direction with similar in-plane grain sizes. Very fine nanotwins were observed in all films with no apparent change in twin density. Ultrahigh compressive yield strengths of 3.1–3.4 GPa were inferred from nanoindentation measurements and found to be invariant over the range of rates. The results indicate that the deposition rate did not have a significant effect on the formation of nanotwins and that alloy chemistry played a more significant role. Alloying with Mo and W appears to reduce the SFE as compared to pure Ni and promotes ubiquitous nanotwin formation. The prolific formation of the nanotwins precludes the use of deposition rate as a means for tailoring spacing or density and attendant mechanical properties, but on the positive side it does provide a wide processing window for making nanotwinned Ni–Mo–W films for metal MEMS applications.

The authors would like to acknowledge Prof. Kelvin Xie for assistance in initial TEM sample preparation and imaging. This study was supported by the Department of Energy Basic Energy Sciences, under grant DE-FG02-07ER46437.

Declaration of Competing Interest

G.M.V., J.A.K., T.P.W and K.J.H. are authors on a patent application in the U.S. (application no. 16/609,968, filed October 31, 2019) and Europe (application no. 1879547.2, filed November 18, 2019) with Japan and Korea in progress. Each of these applications claim priority to PCT/US2018/030384, filed May 1, 2018, which claims priority to U.S. Provisional Patent Application No. 62/492,558 filed by Johns Hopkins Technology Ventures.

Supplementary materials

Supplementary material associated with this article can be found, in the online version, at doi:[10.1016/j.scriptamat.2020.05.031](https://doi.org/10.1016/j.scriptamat.2020.05.031).

References

- [1] G.-D. Sim, J.A. Krogstad, K.M. Reddy, K.Y. Xie, G.M. Valentino, T.P. Weihs, K.J. Hemker, *Sci. Adv.* 3 (6) (2017) e1700685.
- [2] G.-D. Sim, J.A. Krogstad, K.Y. Xie, S. Dasgupta, G.M. Valentino, T.P. Weihs, K.J. Hemker, *Acta Mater.* 144 (2018) 216–225.
- [3] G.M. Valentino, J.A. Krogstad, T.P. Weihs, K.J. Hemker, *J. Alloys Compd.* (2020) 155024.
- [4] G.M. Valentino, P.P. Shetty, J.A. Krogstad, K.J. Hemker, *J. Microelectromech. Syst.* (2020), doi:[10.1109/JMEMS.2019.2958862](https://doi.org/10.1109/JMEMS.2019.2958862).
- [5] M. Dao, L. Lu, Y. Shen, S. Suresh, *Acta Mater.* 54 (20) (2006) 5421–5432.
- [6] L. Lu, X. Chen, X. Huang, K. Lu, *Science* 323 (5914) (2009) 607–610.
- [7] L. Lu, Y. Shen, X. Chen, L. Qian, K. Lu, *Science* 304 (5669) (2004) 422–426.
- [8] K. Lu, L. Lu, S. Suresh, *Science* 324 (5925) (2009) 349–352.
- [9] D.E. Burns, Y. Zhang, M. Teutsch, K. Bade, J. Aktaa, K.J. Hemker, *Scr. Mater.* 67 (5) (2012) 459–462.
- [10] D.E. Burns, Y. Zhang, T.P. Weihs, K.J. Hemker, *Superalloys* (2012) (2012) 569–575.
- [11] J. Li, J. Zhang, L. Jiang, P. Zhang, K. Wu, G. Liu, J. Sun, *Mater. Sci. Eng. A-Struct.* 628 (2015) 62–74.
- [12] S. Dahlgren, W. Nicholson, M. Merz, W. Bollmann, J. Devlin, R. Wang, *Thin Solid Films* 40 (1977) 345–353.
- [13] R. Wang, S. Dahlgren, *J. Mater. Sci.* 10 (8) (1975) 1456–1458.
- [14] Q. Li, S. Xue, P. Price, X. Sun, J. Ding, Z. Shang, Z. Fan, H. Wang, Y. Zhang, Y. Chen, H. Wang, K. Hattar, X. Zhang, *Nanoscale* 12 (3) (2020) 1356–1365.
- [15] O. Anderoglu, A. Misra, F. Ronning, H. Wang, X. Zhang, *J. Appl. Phys.* 106 (2) (2009) 024313.
- [16] L. Velasco, A.M. Hodge, *Acta Mater.* 109 (2016) 142–150.
- [17] L. Velasco, M.N. Polyakov, A.M. Hodge, *Scr. Mater.* 83 (2014) 33–36.
- [18] J.A. Thornton, *J. Vac. Sci. Technol.* 12 (4) (1975) 830–835.
- [19] J.A. Thornton, *Annu. Rev. Mater. Sci.* 7 (1) (1977) 239–260.
- [20] W.C. Oliver, G.M. Pharr, *J. Mater. Res.* 7 (6) (1992) 1564–1583.
- [21] G.M. Valentino, S. Xiang, J.A. Krogstad, L. Ma, K.Y. Xie, T.P. Weihs, K.J. Hemker, (Manuscript in preparation).
- [22] D.E. Burns, Y. Zhang, T.P. Weihs, K.J. Hemker, *Thin Solid Films* 558 (2014) 20–23.
- [23] R. Schwaiger, B. Moser, M. Dao, N. Chollacoop, S. Suresh, *Acta Mater.* 51 (17) (2003) 5159–5172.
- [24] L. Lu, R. Schwaiger, Z. Shan, M. Dao, K. Lu, S. Suresh, *Acta Mater.* 53 (7) (2005) 2169–2179.
- [25] R. Ott, J. Geng, M. Besser, M. Kramer, Y. Wang, E. Park, R. LeSar, A. King, *Acta Mater.* 96 (2015) 378–389.
- [26] S. Shang, C. Zacherl, H. Fang, Y. Wang, Y. Du, Z. Liu, *J. Phys.: Condens. Matter* 24 (50) (2012) 505403.
- [27] N. Bernstein, E. Tadmor, *Phys. Rev. B* 69 (9) (2004) 094116.
- [28] J.P. Hirth, J. Lothe, T. Mura, *Theory of Dislocations*, American Society of Mechanical Engineers Digital Collection, 1983.
- [29] L. Murr, *Scr. Metall.* 6 (3) (1972) 203–208.
- [30] D. Cockayne, M. Jenkins, I. Ray, *Philos. Mag.* 24 (192) (1971) 1383–1392.
- [31] W. Stobbs, C. Sworn, *Philos. Mag.* 24 (192) (1971) 1365–1381.
- [32] X. Zhang, A. Misra, H. Wang, T. Shen, M. Nastasi, T. Mitchell, J. Hirth, R. Hoagland, J. Embury, *Acta Mater.* 52 (4) (2004) 995–1002.